Journal of Inorganic Biochemistry 102 (2008) 1901–1909

Contents lists available at ScienceDirect

Journal of Inorganic Biochemistry

journal homepage: www.elsevier.com/locate/jinorgbio

Structural differences between Pb^{2+}- and Ca^{2+}-binding sites in proteins: Implications with respect to toxicity

Michael Kirberger, Jenny J. Yang *

Center for Drug Design and Biotechnology, Department of Chemistry, Georgia State University, 50 Decatur Street, 550 NSC, Atlanta, GA 30303, United States

ARTICLE INFO

Article history:
Received 7 March 2008
Received in revised form 20 June 2008
Accepted 23 June 2008
Available online 5 July 2008

Keywords:
Metalloprotein
Toxicity
Electrostatic
Opportunistic binding
Misfolding

ABSTRACT

Pb^{2+} is known to displace physiologically-relevant metal ions in proteins. To investigate potential relationships between Pb^{2+}/protein complexes and toxicity, data from the protein data bank were analyzed to compare structural properties of Pb^{2+}- and Ca^{2+}-binding sites. Results of this analysis reveal that the majority of Pb^{2+} sites (77.1%) involve 2–5 binding ligands, compared with 6 ± 2 for non-EF-Hand and 7 ± 1 for EF-Hand Ca^{2+}-binding sites. The mean net negative charge by site (1.7) fell between values noted for non-EF-Hand (1 ± 1) and EF-Hand (3 ± 1). Oxygen is the dominant ligand for both Pb^{2+} and Ca^{2+}, but Pb^{2+} binds predominantly with sidechain Glu (38.4%), which is less prevalent in both non-EF-Hand (10.4%) and EF-Hand (26.6%) Ca^{2+}-binding sites. A comparison of binding geometries where Pb^{2+} has replaced Ca^{2+} in calmodulin (CaM) and Zn^{2+} in 5-aminolaevulinic acid dehydratase (ALAD) revealed protein structural changes that appear to be unrelated to ionic displacement. Structural changes observed with CaM may be related to opportunistic binding of Pb^{2+} in regions of high electrostatic charge, whereas ALAD may bind multiple Pb^{2+} ions in the active site. These results suggest that Pb^{2+} adapts to structurally-diverse binding geometries and that opportunistic binding may play an active role in molecular metal toxicity.

1. Introduction

Complex formation between inorganic metals and proteins is essential to numerous biological processes, where binding of physiologically-relevant metals (e.g. Ca, Mg, Zn, Fe) effects conformational changes that confer new functions. Nearly 40% of all proteins are known to bind metals [1–6]. Metal-binding sites in general are characterized by a central shell of hydrophilic chelating ligands, with a surrounding shell of hydrophobic residues [7,8], and the binding geometry, coordination number, and ligand preference associated with the binding of essential metal ions to natural proteins has been studied extensively [4,9–14].

Ca^{2+}-binding proteins (CaBPs) represent a large family of these metalloproteins. Calmodulin (CaM) is an important CaBP, widely-distributed among eukaryotes, that binds up to four Ca^{2+} ions (Fig. 1a) with continuous EF-hand motifs. The resulting Ca^{2+}-CaM complex mediates biological processes related to inflammation, muscle contraction, memory, nerve growth and the immune response, and may act as a sensor/signal transducer when it binds with proteins unable to bind Ca^{2+} themselves [15,16]. Ca^{2+} may also interact with proteins to regulate functions related to cell division, apoptosis and intracellular signaling [17–20], as well as to enhance protein stability [21].

The coordination chemistry of proteins that facilitates binding of essential metal ions also makes them susceptible to interaction with toxic metals. In addition to Pb^{2+}, Sr^{2+}, Hg^{2+} and Cd^{2+}, most lanthanides have been found to bind with both natural and engineered CaBPs [22–26], and many of these can activate and then inhibit CaM in response to changes in metal concentration, thus altering the activity of downstream CaM-mediated functions [27–32]. Additionally, several recent studies have reported bacterium capable of encoding sensor or chelate proteins for toxic metals [33–35], including *Ralstonia metallidurans*, which possesses the first identified bacterial resistance determinant found to be specific for Pb^{2+} [36].

Despite rigorous studies aimed at understanding the structural implications of metal-binding for physiologically-relevant metals, the binding characteristics of toxic metals like lead (Pb^{2+}) are less clearly defined. Pb^{2+} is a particularly persistent anthropogenic toxicant whose bioavailability has increased as a result of human industry. Physiological effects of Pb^{2+} uptake include neurological disorders, anemia, kidney damage, hypertension and male fertility decrease [37–42]. At the molecular level, Pb^{2+} has been shown to specifically target voltage-gated calcium channels [43]; activate skeletal muscle troponin C (TnC) [44]; and displace both Ca^{2+} and Zn^{2+} in proteins, including CaM, protein kinase C [45],

* Corresponding author. Tel.: +1 404 413 5520; fax: +1 404 413 5551.
E-mail address: chejjy@langate.gsu.edu (J.J. Yang).

0162-0134/$ - see front matter © 2008 Elsevier Inc. All rights reserved.
doi:10.1016/j.jinorgbio.2008.06.014

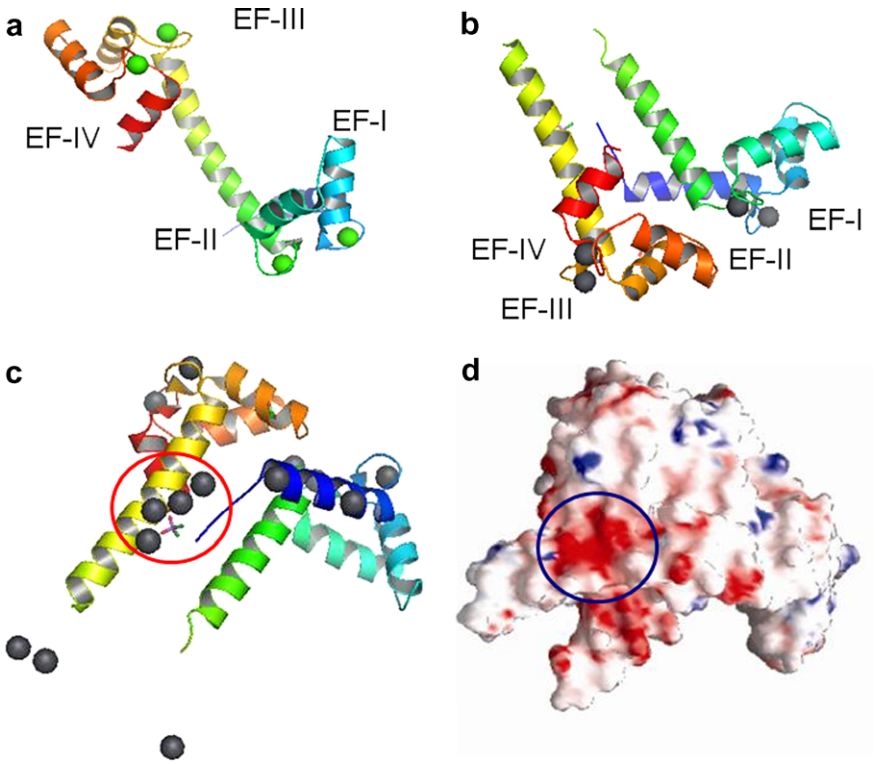

Fig. 1. Proteins 1exr (a), Ca-bound calmodulin, and 1n0y (b), Pb-bound calmodulin. EF-1 through EF-IV are Ca^{2+}-binding sites. (c) Four Pb^{2+} ions (circle) opportunistically bound along groove between chains in 1n0y. (d) Electrostatic potential surface map of 1n0y rendered with GRASP, showing region of negative charge density (circle) where Pb^{2+} ions are bound.

and synaptotagmin [46]. Several studies have indicated that a thiol-rich site binds Pb^{2+} in a distorted trigonal pyramidal geometry with three ligands, or alternatively with a geometry including 5–8 ligands, which differs from reported coordination numbers for Zn^{2+} of either 4–6 or 8 ligands [47–52]. Both carboxyl- and cysteine-rich sites associated with the binding of Pb^{2+} are reported with toxic metal-sensing proteins, where the latter binding sites include 3–4 cysteine residues, arranged in either a distorted tetrahedral or a trigonal coordination geometry [33,35].

To further our understanding of Pb^{2+} toxicity at the molecular level, we report a quantitative analysis of Pb^{2+}-protein complexes listed in the Protein Data Bank (PDB) (http://www.rcsb.org/pdp/) to evaluate structural characteristics associated with binding. Two structures of CaM from the species *Paramecium tetraurelia* (Fig. 1a and b), the only protein currently in the PDB with both Ca^{2+}- and Pb^{2+}-loaded forms, are compared to evaluate physical characteristics associated with binding of the different ions. CaM was specifically analyzed in this study for three reasons. First, it is an essential signaling protein involved in over 100 biological processes and has been studied extensively [53–56]. Second, two significant studies, using different spectroscopic methods, have reported high affinity binding of Pb^{2+} in CaM [57,58]. This potential for high affinity binding in concert with the essential role of calmodulin involved in various biological processes and calcium signaling may represent an important link to Pb^{2+} toxicity at the molecular level which can be revealed through detailed structural analysis. Third, CaM contains four EF-hand motifs. First described by Kretsinger in 1973 [59], this common Ca^{2+}-binding motif found in more than 50% of all CaBPs is characterized by a sequence of approximately 30 amino acids arranged in a helix-loop-helix structure with a pentagonal-bipyramid geometry (Fig. 2a) [60,61]. Recent work in our lab has confirmed the displacement of Ca^{2+} by Pb^{2+} in isolated CaM loops [M. Kirberger and J.J. Yang, manuscript in preparation]. A similar structural analysis using PDB data was also completed with two structures of yeast 5-aminolaevulinic acid dehydratase (ALAD) bound with Zn^{2+} and Pb^{2+}.

Analysis of data presented in this study led us to hypothesize that while ionic displacement of Ca^{2+} by a competing metal ion may represent one mechanism of metal toxicity, an additional opportunistic binding mechanism, resulting from metal–protein interactions in regions lacking an established binding site and related to electrostatic potential interactions, may represent an additional avenue for metal toxicity. Both mechanisms may offer partial explanations for the activation/inhibition of CaM activity reported in related studies [27–32].

2. Materials and methods

A preliminary search of the Protein Data Bank identified 27 PDB files for proteins known to bind Pb^{2+}. Six of these were discarded as they represented either duplicate structures or nucleic acid structures. From the remaining 21 PDB files, 20 of the 68 Pb^{2+} binding sites were eliminated due to redundancy associated with polymeric domains, or because the only binding ligands associated with the ion were water molecules, leaving 48 binding sites retained for the analysis (Table S1).

Although possible Pb–O and Pb–N binding distances as long as 4.2 Å have been reported in the literature [62], we chose a shorter ligand inclusion cutoff distance of 3.5 Å from the Pb^{2+} ion for several reasons. First, 75% of the ligands identified by the analysis fell within the 3.5 Å cutoff distance, including all of the ligands where binding resulted from displacement of another ion. Second, work by Harding and others [62,63] has suggested a variable region approximately between 3.2–4.0 Å where the distribution of ligands for certain metal ions decreases significantly, and begins to increase again near 4.0 Å. This corresponds with second shell interac-

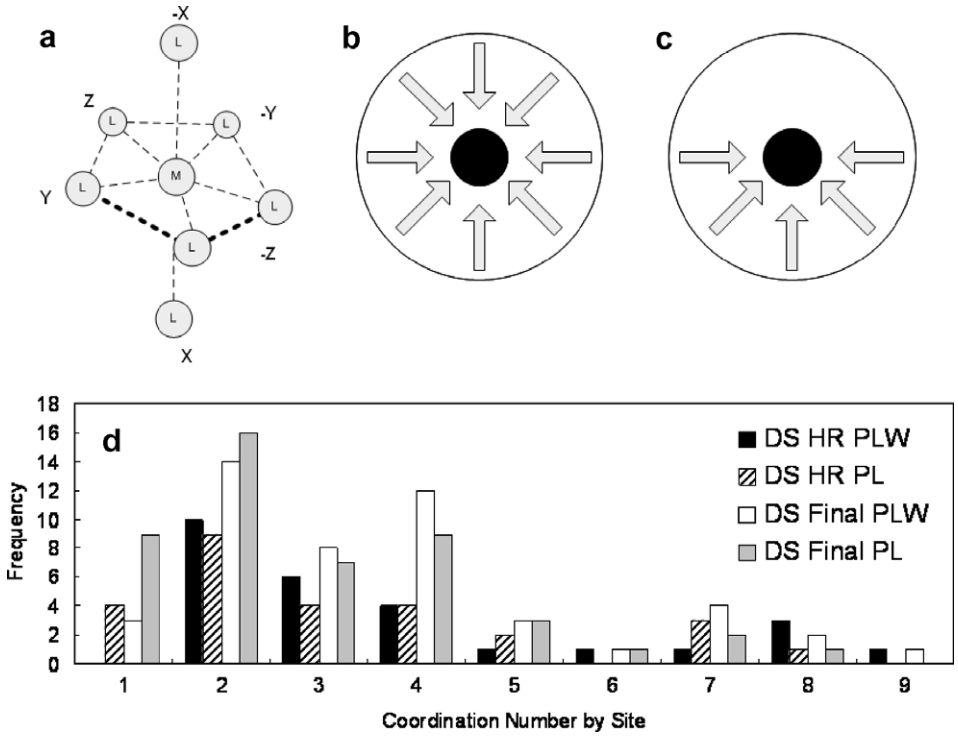

Fig. 2. (a) Pentagonal-bipyramidal geometry typical of well-ordered EF-Hand Ca^{2+}-binding site. (b) Holodirected and (c) hemidirected binding coordination schemes for Pb^{2+} proposed by Shimoni-Livny et al. [70]. (d) Frequency distribution of CN values, with and without water, for DS HR and DS Final.

tion ranges reported by Dudev [11], where first shell interactions are constrained to 3.5 Å. This cutoff distance is also frequently cited as the upper limit for Ca^{2+} binding; however, nearly all studies of Ca^{2+}, including a recent study completed in our laboratory, have demonstrated that Ca^{2+}-binding ligands are generally within 2.9 Å distance from the ion [4,10,63,64]. In the case of Pb^{2+} which has a slightly larger radius than Ca^{2+}, we allowed for the possibility that the larger radius would result in minor increases in binding distance values, which is accommodated by the 3.5 Å cutoff.

Of the 177 ligand atoms retained for the analysis, only five have occupancy values less than 1 (i.e. more than one stable set of coordinates was observed for the atom in the crystalline structure), and these atoms were not removed as their inclusion would not significantly alter the analysis. Two datasets were then constructed for evaluation: a final dataset (DS Final) comprised of all retained binding sites, and a subset comprised of higher resolution (DS HR) structural data (R less than 1.76 Å), to limit error inherent in structures with lower resolution [65].

Data from the ligand protein contact data server (LPC) (http://bioportal.weizmann.ac.il/oca-bin/lpccsu) were obtained to verify binding ligands. Data from the PDB were selectively filtered using a custom, Visual Basic (Microsoft Corporation, Redmond, WA) program, then loaded into an Access relational database. Statistical data on binding ligands were extracted from the database using Structured Query Language (SQL) queries to identify all potential oxygen, nitrogen or sulfur ligand atoms within 3.5 Å of the target Pb^{2+} ions. Distance was calculated based on Eq. (1), where $(X_{Ligand} - X_{Pb})$ indicates the spatial difference between each component's numerical coordinate along the X-axis. The differences for each component along the Y- and Z-axis are calculated in the same manner.

$$\text{Distance} = \left(\left(X_{Ligand} - X_{Pb}\right)^2 + \left(Y_{Ligand} - Y_{pb}\right)^2 + \left(Z_{Ligand} - Z_{pb}\right)^2 \right)^{1/2}. \quad (1)$$

Additionally, 54 potential bidentate ligand pairs in the PDB files were inspected using Pymol [66], and 36 were visually-identified as bidentate pairs. For these, a bidentate ligand propensity property L_β (Eq. (2)) was defined based on the ratio (d_1/d_2) where d_1 represents the distance between Pb^{2+} and either Asp OD1 or Glu OE1, and d_2 represents the distance between Pb^{2+} and either Asp OD2 or Glu OE2.

$$L_\beta = (d_1/d_2). \quad (2)$$

The geometric ratio (d_1/d_2 or L_β) describes the deviation from unity for a theoretically-symmetric bidentate ligand group. This deviation increases as the denticity moves from bidentate to monodentate. Because d_1 may be either greater than or less than d_2, calculation of L_β for multiple bidentate ligands produces a value range with a central point near 1 (i.e. unity). The L_β range determined for Pb^{2+}-binding was found to be 1.04 ± 0.29, which differs from that calculated for Ca^{2+} (1.07 ± 0.34), and we expect to observe small, metal-specific variations. The significance of this property is that it can be utilized in related analyses to predict bidentate ligands from structural data, without the necessity of viewing each individual model. Further detailed information describing the empirical derivation of this property is described in a related publication [M. Kirberger and J.J. Yang, manuscript in preparation].

Comparative data for Ca^{2+}-binding was also obtained from the Protein Data Bank, where a total of 1605 binding sites from 558 PDB files with resolution $R \leqslant 2.0$ Å were retained for the analysis, based on a cutoff distance of 3.5 Å as the maximum ligand distance for oxygen and nitrogen, and following removal of structures with greater than 90% sequence homology.

3. Results and discussion

Table S2 lists the retained binding sites, their PDB identifiers, coordination number (CN) values both with (PLW) and without (PL) water molecules, formal charge (FC), and binding mode (D – displacement, O – opportunistic, or U – unknown) by site. As seen in Table S2, approximately 1/3 of the Pb^{2+}-binding sites were

identified as sites of ionic displacement, indicating that these sites are also known to bind physiologically-relevant ions, as listed in the Binding column. Statistical analysis of these two separate binding modes was not performed in this study due to limited data for each of the different metals listed.

Binding sites from the high-resolution dataset (DS HR) are identified by an asterisk preceding the PDB_ID. A charge of (−1) was assigned to acidic sidechain ligands Glu and Asp, and the Cys thiol [67]. Table 1 presents a summary of all statistical data from the analysis. A comparison of the values reported for DS HR and DS Final shows little difference in ligand distance values, coordination number, and charge, indicating that resolution did not significantly alter the results. Consequently, unless otherwise specified, results from only the DS Final dataset are discussed from the analysis. These statistical results for Pb^{2+} are then compared with data recently compiled for Ca^{2+} to emphasize differences in binding characteristics exhibited by the two metals.

3.1. Ligand coordination by binding site

The coordination numbers presented in Table 1 are differentiated based on the inclusion or exclusion of water oxygen ligands. For the DS Final dataset, mean CN values were reported as 2.9 ± 1.7 and 3.7 ± 2.0 for the exclusion (PL) and inclusion (PLW) of water ligands, respectively. As reported in this study, ligands (e.g. carboxyl groups) are monodentate unless specifically identified as bidentate, i.e. comprising two ligand atoms. Water occupancies in the crystalline structures are considered approximations. The distribution of CN by site (Fig. 2d) indicates that binding was most commonly observed with two, or to a lesser extent, four ligands. Interestingly, nine sites were reported with only a single amino acid ligand atom for coordination when water was excluded, and three of these were unchanged even with the inclusion of oxygen ligands from water.

The distribution of CN values in Table 1 is further divided into percentages falling between the ranges of 2–5 ligands (77.1%) and 6–9 ligands (16.7%). The CN range of 2–5 was selected for two reasons. First, previous studies have indicated that Pb^{2+} may adopt a binding structure similar to Zn^{2+}, using 4–6 binding ligands, as a result of ionic displacement [68,69]. Second, a study of crystalline structure data in the Cambridge Structural Database by Shimoni-Livny et al. [70] observed two general geometries for Pb^{2+}-binding: a holodirected, spherical geometry comprised of 9–10 ligands (Fig. 2b) and a hemidirected geometry where 2–5 coordination ligands occupy only half of a sphere (Fig. 2c). It is notable that a hemidirected or planar geometry was also observed in nearly 28% of the Non-EF-Hand Ca^{2+} binding sites surveyed in our recent statistical analysis [M. Kirberger and J.J. Yang, manuscript in preparation], indicating that this geometry is not confined to Pb^{2+}-binding.

Alternatively, the CN range of 6–9 was selected both for comparison with Ca^{2+}-binding (6–8 ligands) [71] and because previous studies with small molecules suggested a coordination number of 6.9 for Pb^{2+} [4]. The results of this analysis indicate that binding coordination of Pb^{2+}, based on number of ligands, is more closely-related to that of Zn^{2+} than Ca^{2+}. This is particularly apparent with respect to the EF-Hand Ca^{2+}-binding sites which average 6–8 ligands in well-ordered structures. These results, which conflict with conclusions reported from studies of small molecules, are, however, consistent with hard-soft acid models for metals. Ca^{2+} is classified as a hard Lewis acid (Table S3) with an ionic radius of 0.99–1.12 Å for a typical coordination number of 6–8 based on studies of small molecules [4,19]. Conversely, Pb^{2+} has a reported ionic radius of 1.12–1.19 Å for similar coordination. Both Pb^{2+} and Zn^{2+} are classified as borderline acids, exhibiting properties of both hard and soft acids, so it is reasonable to assume that Pb^{2+} may share more similar binding features with Zn^{2+} than Ca^{2+}.

Table 1
Pb^{2+}-binding statistics

	DS HR	DS Final
Total PDB proteins in study	7	21
Total Pb binding sites evaluated	27	48
Total target ligand atoms	105	177
Total O_{aa} ligands	86	118
Total O_{HOH} ligands	16	36
Total N ligands	3	10
Total S ligands	0	13
Total sites with N ligands	3	9
Mean CN, PLW	3.9 ± 2.3	3.7 ± 2.0
% CN 2–5	77.8	77.1
% CN 6–9	22.2	16.7
Mean CN, PL	3.3 ± 2.0	2.9 ± 1.7
% CN 2–5	70.4	72.9
% CN 6–9	14.8	8.3
Mean charge by site	−1.8	−1.7
Total identified bidentate pairs	24	36
Total sites with bidentate ligands	21	30
% Sites with bidentate ligands	77.8	62.5
Mean distance, Pb–O_{aa}, (Å)	2.7 ± 0.4	2.7 ± 0.4
Mean distance, Pb–O_{HOH}, (Å)	2.8 ± 0.3	2.8 ± 0.4
Mean distance, Pb–N (Å)	2.7 ± 0.3	2.6 ± 0.4
Mean distance, Pb–S (Å)	–	3.2 ± 0.3

DS HR: high-resolution dataset (less than 1.76 Å), 3.5 Å ligand atom distance cutoff. DS Final: summary dataset, no restriction on resolution, 3.5 Å ligand atom distance cutoff, refined for bidentate ligands. CN: coordination number. PLW: ligands from protein and water. PL: ligands from protein only. O_{aa}: amino acid oxygen ligand. O_{HOH}: water oxygen ligand.

3.2. Charge by binding site

The relative % distribution of charge between the two datasets is shown in Fig. 3a, indicating a range from 0 to −4 in the binding site, with a mean negative charge of 1.7 ± 1.1 for DS Final (Table 1). The mean and net charge values reported for the metal binding sites do not reflect positive charge contribution from the divalent cation. Previous studies of Ca^{2+} have indicated that higher binding affinities are found with a net negative charge within 5–15 Å of the ion [72,73], and a microenvironment containing 3–4 negative charges likely represents an optimal charge configuration [67,74]. However, a more recent study in our laboratory indicates that this is representative of the more highly-structured EF-Hand proteins. The rounded net negative charge for Pb^{2+}-binding sites (2 ± 1) falls between the structurally more diverse Non-EF-Hand proteins (1 ± 1) and the EF-Hand proteins (3 ± 1). Charge interactions for Pb^{2+} are likely stabilized due to the higher electronegativity (Table S3) and increased potential for partial covalent bond formation of Pb^{2+}, so that it is less structurally-constrained and can bind more opportunistically than Ca^{2+}.

3.3. Binding ligands

Oxygen atoms from amino acids represent the major binding ligand for Pb^{2+} (118), followed by oxygen from water (36), sulfur (13) and nitrogen (10) (Table 1). The % relative distribution of ligand atoms shown in Fig. 4a indicates that binding ligand preference for Pb^{2+} followed the order sidechain Glu (38.4%) > sidechain Asp (20.3%) = water (20.3%) > Sulfur (7.3%). For comparison, the distributions of ligand preference for EF-Hand and Non-EF-Hand Ca^{2+}-binding proteins are presented in Fig. 4b and c, respectively. From these figures, it can be seen that Pb^{2+} differs in several significant ways from Ca^{2+}-binding. The increased use of sidechain Glu by Pb^{2+} (38.4%) followed by sidechain Asp (20.3%) contrasts sharply with trends observed in both the

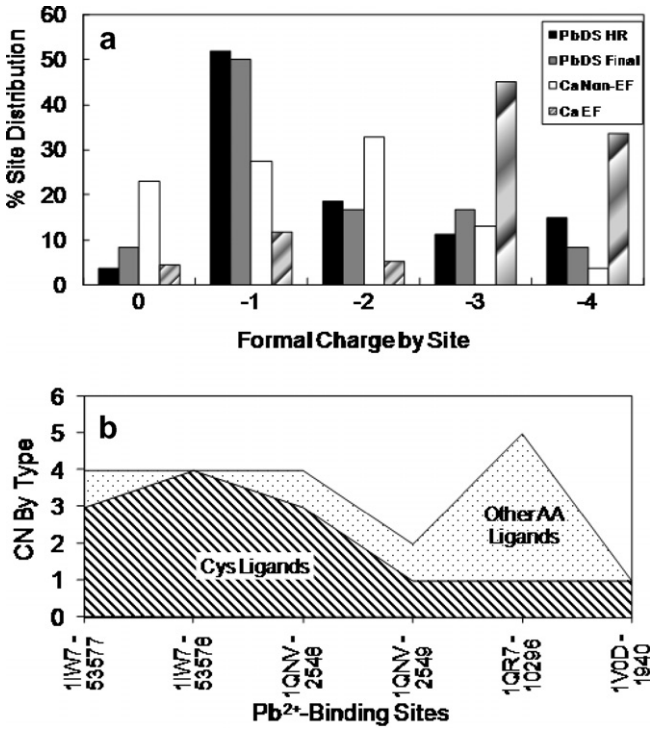

Fig. 3. (a) Relative % distribution of charge values for Pb^{2+}-binding sites from DS HR and DS Final, and Ca^{2+}-binding sites for Non-EF-Hand and EF-Hand proteins. (b) Distribution of CN values by type for six Pb^{2+}-binding sites containing sulfur ligands. Other AA in the figure represents ligand atoms other than sulfur from amino acids. Abscissa labels indicate PDB file ID and serial number for Pb^{2+} ion.

highly-structured EF-Hand sites (sidechain Asp, 29.7%; sidechain Glu 26.6%) and the more structurally-diverse Non-EF-Hand sites (sidechain Asp, 24.5%; sidechain Glu, 10.4%). The presence of water in the Pb^{2+} sites falls roughly in the middle of the two Ca^{2+}-binding classes, but utilization of carbonyl oxygen atoms by Pb^{2+} is considerably lower than both the EF and Non-EF Ca^{2+}-binding classes (Fig. 4).

Table 1 also summarizes the mean binding distance values determined from the analysis. The Pb–O distance (for amino acids) was found to be 2.7 ± 0.4 Å, which is slightly higher than the mean of 2.4 ± 0.2 Å reported for Ca–O. The mean distances reported for Pb–O (water), Pb–N and Pb–S were 2.8 ± 0.4 Å, 2.6 ± 0.4 Å, and 3.2 ± 0.3 Å, respectively. Except for Pb–S, these values were nearly identical despite expectations that Pb–N would exhibit a longer binding distance based on a comparison with data from Sarret et al. [62], where ranges for Pb–O, Pb–N and Pb–S were reported as 2.2–4.2 Å, 3.0–4.2 Å, and 2.6–3.4 Å, respectively.

Nitrogen is generally accepted as a binding ligand for Pb^{2+}, and marginally for Ca^{2+}, with small molecules; however, in our detailed statistical analysis of protein calcium binding sites [M. Kirberger and J.J. Yang, manuscript in preparation], less than 1% of all identified potential ligands were nitrogen atoms, and the limited contribution by nitrogen to bind Pb^{2+} in proteins is clear in Fig. 4a. Only ten nitrogen atoms were identified as potential ligands within a cutoff distance of 3.5 Å. Nine of these were from sidechains, with six from His, two from Lys and one from Gln. Although the low pK_a (6.0) for His makes it a suitable binding ligand, Lys is unlikely to function as a binding ligand as its pK_a is significantly higher than physiological pH. For Gln, and presumably Asn, it is more likely to assume that binding of Pb^{2+} would occur with the polar, uncharged $-CO(NH_2)$ functional group, rather than the isolated sidechain nitrogen, due to the conjugated π-bond system and the planar structure of the group resulting from resonance. It can be inferred from these data that nitrogen plays a more limited role in the binding of Pb^{2+} to proteins than what has been reported in the case of small molecules.

Additionally, since Pb^{2+} was previously reported by Magyar and Andersen [47,52] to bind in a thiol-rich site with a tendency to adopt a three ligand, trigonal pyramidal geometry, we attempted to evaluate the limited data available for sulfur ligands. As shown in Fig. 3b, data were available for only six Pb^{2+}-binding sites which included sulfur ligands, where coordination number values reported were 1, 2, 4 and 6, with binding by four ligands apparent

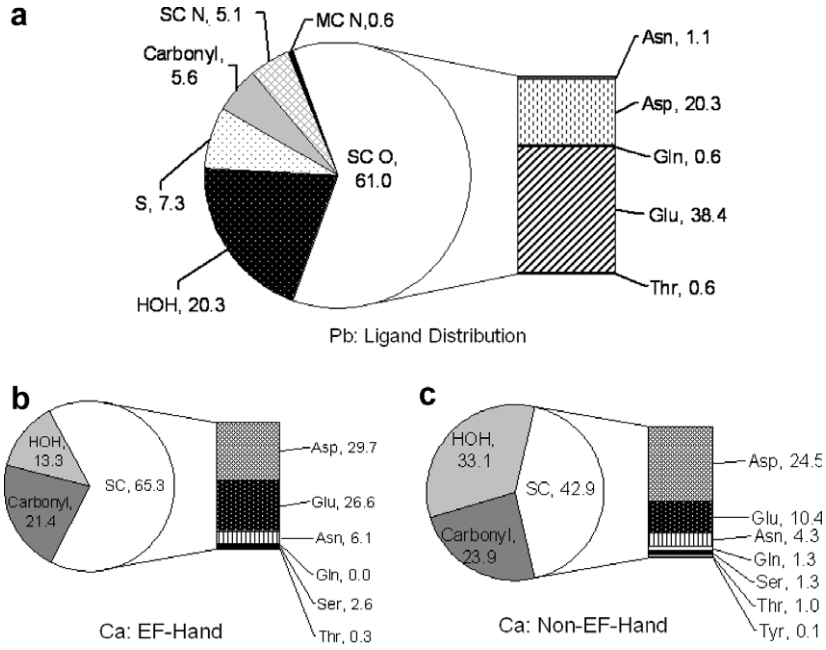

Fig. 4. Percent distribution of ligands for (a) Pb^{2+}, (b) EF-Hand Ca^{2+} and (c) non-EF-Hand Ca^{2+} binding sites, where: SC indicates sidechain; MC indicates mainchain; O, N, S indicates oxygen, nitrogen, and sulfur, respectively, and; HOH represents ligand oxygen from water.

in three of the six sites. A trigonal pyramidal geometry for Pb^{2+} was not observed in our study; however this may be due to fact that the structures in our limited dataset were not identical to those reported by Magyar and Andersen.

3.4. Structural analysis

Next we evaluated structural changes associated with the displacement of Ca^{2+} by Pb^{2+} in the EF-Hand protein CaM. CaM, like most EF-Hand proteins, exhibits an irregular pentagonal-bipyramidal geometry (Fig. 2a), with five planar ligands at $-Z$, Y, Z, and $-Y$, where $-Z$ is a bidentate ligand. Ligands at X and $-X$ are typically oxygen atoms from a sidechain carboxyl group and a bound water molecule, respectively. CaM also has high sequence similarity between species. An alignment for PDB proteins 3cln, 1exr, and 1n0y using ClustalW (http://www.ebi.ac.uk/clustalw) indicates that the Ca^{2+}- and Pb^{2+}-bound complexes of CaM (1exr.pdb and 1n0y.pdb) share 100% sequence similarity except for an additional Ala at the N-terminal, and a Lys at the C-terminal in 1n0y, and both are 88% homologous to 3cln (Supplementary Fig. S1). The structures of Ca^{2+}-CaM (1exr) and Pb^{2+}-CaM (1n0y) in Fig. 1a and b, respectively, were compared by Wilson et al. [75], who reported a C^{α} RMSD of 2.1 Å in the N-terminal domain compared with 1.1 Å in the C-terminal domain, with the most apparent deviation occurring between the N-terminal helix A and the C-terminal half of helix D/E. Additionally, Fig. 1c shows that 14 Pb^{2+} ions are bound in the crystalline structure of CaM (1n0y), such that Pb^{2+} ions have not only replaced Ca^{2+} ions in the binding pockets, but have also become bound to surface ligands.

The pronounced global conformational changes observed in Fig. 1c for Pb^{2+} bound CaM indicate new folding that is not observed in the Ca^{2+} bound form. An electrostatic potential surface map of protein 1n0y generated using DelPhi and GRASP (Fig. 1d) [76–79] shows an area of concentrated negative charge in the folding groove between Chains A and B where the 4 Pb^{2+} ions appear bound in the structure. However, the backbone RMSD comparing sites EF-I through EF-IV in the two structures, calculated using Sybyl software (Tripos, St. Louis, MO), indicated RMSD values ranging from 0.12 Å in EF-III, to 0.35 Å in EF-IV (Table 2). This suggests minimal disruption of the site due to ion displacement. To further validate this, a Ramachandran plot generated by VADAR [80] for 1n0y revealed that all dihedral angles fall within allowed regions, indicating no apparent strain on the backbone associated with binding of Pb^{2+}. The limited perturbation in the binding sites and the secondary binding of Pb^{2+} coincident with regions of high electrostatic potential strongly suggest that the observed conformational changes are independent of ion displacement, but related instead to our proposed mechanism of opportunistic binding which would imply much stronger binding affinity for the Pb^{2+} ions than what is typically observed with low affinity, non-specific binding of metals at high concentrations.

Consistent with this, a comparison of paired models (Fig. 5: ab, cd, ef, gh) corresponding to EF sites I–IV for Ca^{2+}-binding and Pb^{2+}-binding indicates that the basic geometry for binding of Ca^{2+} is conserved upon binding with Pb^{2+}, and the same binding ligands, with minor exceptions, are used by both ions (Table S4). A comparison of distance and angle values for binding ligands utilized by both ions (Table S4) shows a negligible, mean net increase in the binding distance (0.08 Å) and a corresponding mean sum decrease in the C-Lig-Ion angle (−5.00°) for Pb^{2+}, but the monodentate and bidentate carbon-ligand-ion angles were nearly identical, and in both cases, the mean differences fall within the range of the standard deviation, so they are in all probability not statistically different. The data associated with the bidentate dihedral angles for Ca^{2+}-binding, as summarized in Table 2, correlate well with research reported by McPhalen [81] that indicated a mean distance of 0.4 Å for the Ca^{2+} ion out of the carboxylate plane, with a φ angle under 30°. For Pb^{2+}, however, the mean average distance for the ion increases to 1.00 ± 0.31 Å from 0.21 ± 0.15 Å observed for Ca^{2+}, and the mean bidentate ligand dihedral (φ) angle was much larger for the Pb^{2+} ion (19.92 ± 5.93°) than for Ca^{2+} (4.17 ± 2.98°) (Fig. 6a).

Mean values of 6 and 7 coordination ligands (excluding water) were found for Ca^{2+} and Pb^{2+}, respectively (Table 2), indicating that Pb^{2+} may take advantage of additional proximate ligand oxygen atoms when available, without disruption to the binding site. Nitrogen atoms potentially available as sidechain ligands in the binding loop sequence (Asn60 and Asn97; Figs. 5d and f, respectively) do not appear to be involved in binding, although there are no apparent barriers restricting rotation of the amide group around the C^{γ}–C^{β} bond. This may, however, be due to mislabeling of atoms in the original structure.

For comparative purposes, two structures of yeast 5-aminolaevulinic acid dehydratase (ALAD) from *Saccharomyces cerevisiae* bound with Zn^{2+} (1eb3.pdb) and Pb^{2+} (1qnv.pdb) were also evaluated for changes associated with ionic displacement by Pb^{2+} (Fig. 6). ALAD is a 280-kDa protein comprised of eight identical subunits that each bind a single Zn^{2+} ion. A single subunit from Chain A is presented in PDB files 1eb3 and 1qnv. Previous work by Bergdahl identified ALAD as the protein binding Pb^{2+} in human erythrocytes, where 99% of free Pb^{2+} concentrates in the blood [82], and the relationship between Pb^{2+} toxicity and human ALAD has been well-established [83].

Data from a structural analysis are summarized in Table S5, which demonstrates strong similarity to changes observed in the EF-Hand binding sites for CaM. Distortion of the binding site is observed based on a mean increase in the binding distances of the

Table 2
Summary of angle/distance values for 1exr and 1n0y

	EF-I	EF-II	EF-III	EF-IV	Mean
1EXR total Ca^{2+} ligands	6	6	6	6	6
1N0Y total Pb^{2+} ligands	7	8	6	7	7
Mean sum Δ binding distance Ca → Pb (Å)	0.14	0.08	0.01	0.08	0.08
Mean sum Δ CLI angle Ca → Pb (°)	−8.67	−5.38	−1.34	−4.62	−5.00
RMSD by site (Å)	0.28	0.28	0.12	0.35	0.26 ± 0.10
Ca^{2+} planar monodentate LIL angles (°)	78.14 ± 3.34	78.05 ± 3.08	77.07 ± 1.75	78.76 ± 1.59	78.00 ± 2.37
Pb^{2+} planar monodentate LIL angles (°)	78.95 ± 5.86	75.80 ± 4.74	77.12 ± 2.00	78.70 ± 5.89	77.64 ± 4.57
Ca^{2+} planar bidentate LIL angles (°)	53.01	51.48	52.30	52.35	52.29 ± 0.63
Pb^{2+} planar bidentate LIL angles (°)	50.84	46.49	51.77	48.99	49.52 ± 2.33
Ca^{2+} ion Dihedral (°)	4.91	4.12	7.43	0.23	4.17 ± 2.98
Pb^{2+} ion dihedral (°)	20.76	26.03	21.10	11.79	19.92 ± 5.93
Distance of Ca^{2+} ion out of bidentate plane	0.24	0.21	0.37	0.01	0.21 ± 0.15
Distance of Pb^{2+} ion out of bidentate plane	1.01	1.36	1.02	0.61	1.00 ± 0.31

CLI: carbon-ligand-ion. LIL: ligand-ion-ligand.

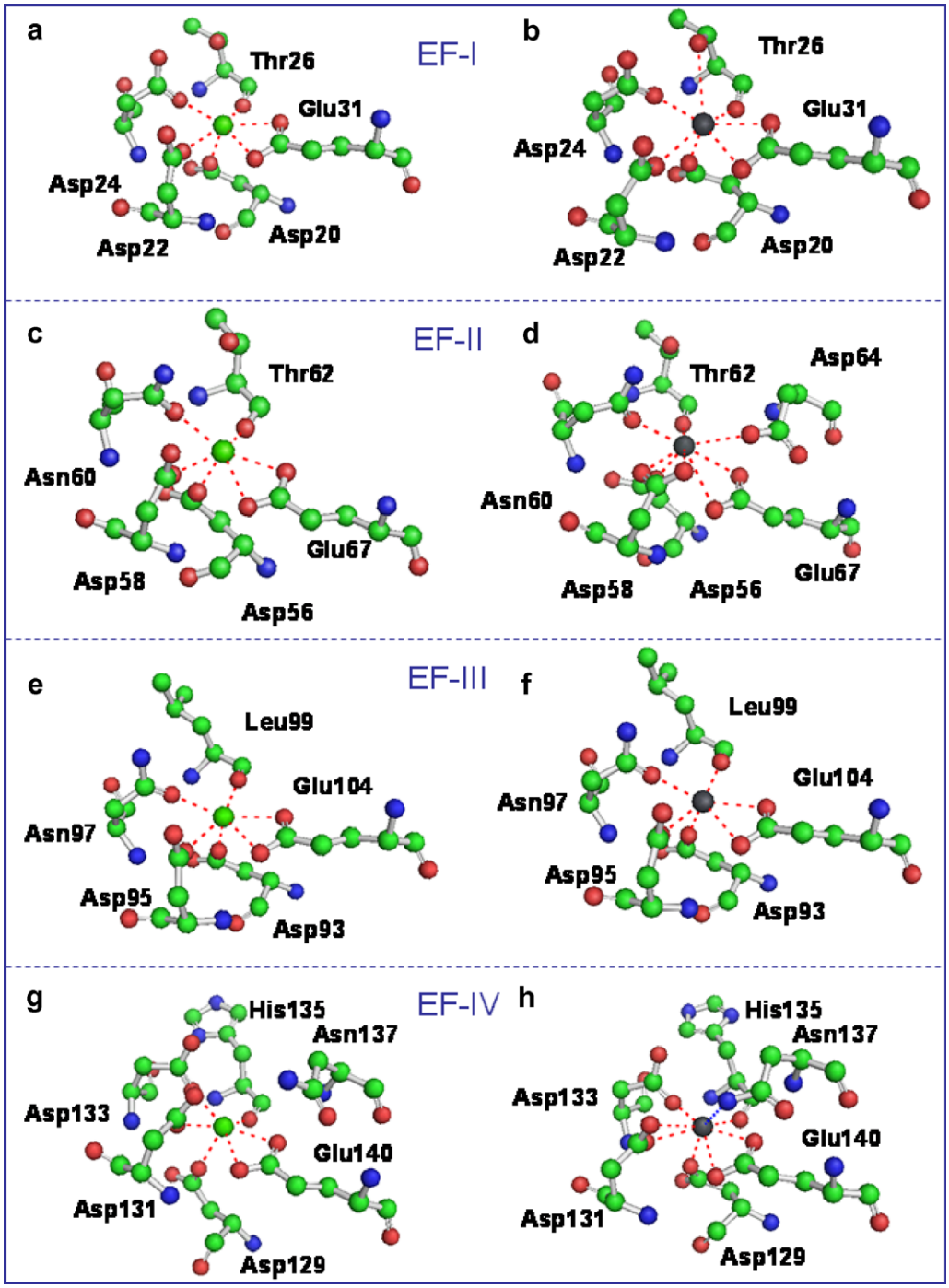

Fig. 5. Paired binding sites EF-I (a, b) EF-II (c, d) EF-III (e, f) and EF-IV (g, h) for PDB proteins 1exr (left) and 1n0y (right).

three Cys thiol ligands (0.54 Å) and decreasing carbon-ligand-ion (CLI) angles for Cys133 and Cys135 (Table S5) which is consistent with the larger radius of Pb^{2+}. Additionally, the carbonyl oxygen of Ser179 which does not appear to be a binding ligand for Zn^{2+} (Fig. 6d, top) is reoriented 0.9 Å to interact with the Pb^{2+} ion (Fig. 6d, bottom). The binding site is formed in a deep pocket where interestingly, a second Pb^{2+} ion is bound 4.40 Å from the ion occupying the binding site, sharing the SG sulfur ligand from Cys143, whereas only a single Zn^{2+} ion is bound in the 1eb3 ALAD structure. Generation of an electrostatic potential map with Sybyl did not indicate dense charge clustering in this region, possibly due to the buried nature of the site.

Erskine et al., who deposited the structure 1qnv.pdb, reported a RMSD value of 0.4 Å for 326 matched C^{α} atoms [84]. Calculations with Sybyl for the resolved structural region indicated a backbone RMSD of 0.58 Å for the structure comprising residues 133–179 and a backbone RMSD value of 1.43 Å for the structure comprising residues 1–219. As was seen with the displacement of Ca^{2+}, disruption of the backbone in the binding site microenvironment appeared minimal as a result of Pb^{2+}-binding.

Based on the results of our analysis, Fig. 6 illustrates characteristics of a proposed model showing the differences between Ca^{2+} and Pb^{2+} during binding. In this model, which includes parameters that may be extensible to Zn^{2+}-binding sites, the slightly larger

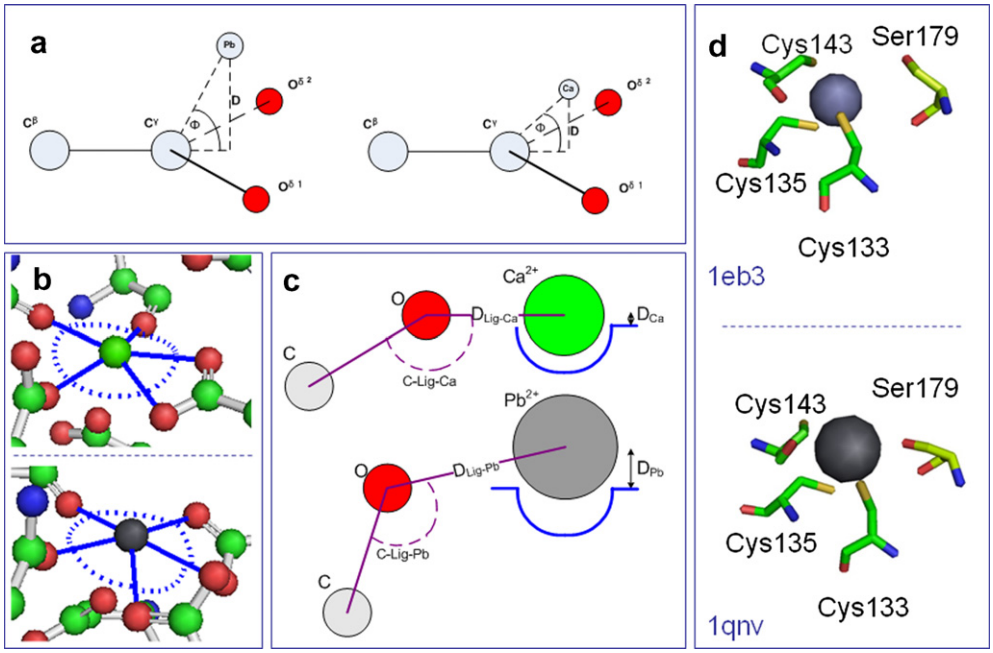

Fig. 6. (a) Illustration of position of the Pb^{2+} ion (left) and the Ca^{2+} (right) with respect to the carboxlyate bidentate plane. D and φ indicate distance and angle of ion relative to plane formed by C^{γ}, $O^{\delta 1}$ and $O^{\delta 2}$. (b) Positions of Ca^{2+} ion (top) and Pb^{2+} ion (bottom) with respect to pentagonal plane. (c) Example illustrating comparison of Ca^{2+}- and Pb^{2+}-binding characteristics with respect to the pentagonal plane. D_{Ca} and D_{Pb} indicate ion distance out of pentagonal plane. (d) Comparison of a binding site from ALAD protein showing Zn^{2+}-binding in 1eb3.pdb (top) and Pb^{2+}-binding in 1qnv (bottom) where one additional ligand (Ser179) is provided for binding of Pb^{2+}.

ionic radius of Pb^{2+} is accommodated by small changes in sidechain ligand orientations, increased displacement of the ion (D_{Pb}) relative to the Ca^{2+} occupancy (D_{Ca}) of the site (Fig. 6c), and more pronounced reorientation of the Glu anchor at $-Z$ (Fig. 6a). This would account for the apparent minimal distortion in the pentagonal plane (Fig. 6b) and more significantly, the backbone. This proposed model accounts for the larger ionic radius of Pb^{2+}, minor rotation of the sidechains, the net increase in binding distance and net decrease in bond angles when binding Pb^{2+} (Table 2), and the increase observed in the bidentate ligand dihedral (φ) angle for the Pb^{2+} ion. It is also consistent with previously-noted observations indicating that Pb^{2+} initially activates then deactivates CaM with increasing Pb^{2+} concentration, where activation of CaM results from ionic displacement, followed by strong opportunistic binding to effect conformational changes.

4. Conclusions

It is apparent from both the structural and database analyses of Pb^{2+}-binding sites that oxygen is the dominant binding ligand for Pb^{2+}, or sulfur in the case of Zn^{2+}-binding sites, with only negligible interaction between Pb^{2+} and nitrogen. The Pb^{2+} binding sites were significantly different from those observed for EF-Hand proteins, requiring fewer coordinating ligands and less negative charge, but sharing more structural similarity with the more disordered Non-EF-Hand sites. Conversely, the increased utilization by Pb^{2+} of Glu (38.4%) over Asp (20.3%) reverses the trend observed for Non-EF-Hand CaBPs (10.4% and 24.5%, respectively), indicating differences in the two binding models not accounted for solely by ionic charge and atom type. Moreover, the significant structural alterations in CaM appear to be due to binding of Pb^{2+} in regions of high surface negative charge potential (Fig. 1c), rather than exchange of Ca^{2+} with Pb^{2+}, which is supported by the low RMSD values reported for ionic displacement (Table 2). The combination of these results, and previous studies citing the initial activation and subsequent inhibition of CaM as a function of toxic metal concentration [27–32], argues that strong opportunistic binding, either coupled with, or independent of, ionic displacement, has several important ramifications with respect to toxicity. First, proteins may bind both opportunistically and by ionic displacement, resulting in activation or inhibition of the protein as a function of metal concentration. Studies of CaM showing initial activation followed by inhibition in response to increasing concentration of metal ion (e.g. Pb^{2+}) suggests that initial binding in the active sites may first activate the protein as if bound with Ca^{2+}, but the subsequent deactivation may result from more pronounced conformational changes resulting from additional opportunistic binding. Second, strong non-specific or opportunistic binding can potentially increase solubility and facilitate transport and diffusion of toxic metals, as may be the case with ALAD from human blood erythrocytes, which may potentially bind multiple Pb^{2+} ions in a site normally occupied by a single Zn^{2+} ion.

Furthermore, the apparent, promiscuous binding of Pb^{2+} is suggested by the variety of ions it can displace (Table S2), its adaptability to different coordination geometries, and the wide range of coordination numbers and charge values associated with opportunistic binding in the absence of well-defined binding sites. Additionally, recently reported studies indicate that bacterial proteins encode different binding motifs in sensors capable of detecting Pb^{2+}. CmtR, a Cd^{2+}/Pb^{2+} regulator expressed in *Mycobacterium tuberculosis*, binds Pb^{2+} with three Cys thiols, more typical of Zn^{2+} binding [85]. However, in *Ralstonia metallidurans* strain CH34, a Cys ligand is replaced by two Glu residues, resulting in a binding motif more similar to that of Ca^{2+} [36]. It is presumed that the ability of Pb^{2+} to bind opportunistically may extend to non-metalloproteins, thus increasing the number of potential target proteins whose function may be altered due to the introduction of toxic metals.

5. Abbreviations

CaBP	calcium-binding protein
CaM	calmodulin
CN	coordination number
DS	dataset
FC	formal charge
HR	high-resolution
LPC	ligand protein contact data server
PDB	Protein Data Bank
PL	protein ligands
PLW	protein ligands and water
RMSD	root-mean-squared deviation

Acknowledgements

The authors would like to thank Dr. Wei Yang from NIH for helpful suggestions, and Ning Chen, Dr. Jin Zou and Dan Adams for their critical review of the manuscript. Thanks also to Dr. Hsiau-Wei Lee and Jie Jiang for helpful instructions on the use of Sybyl and DelPhi software. Special thanks to Dr. Robert Kretsinger for his very helpful review, comments and criticisms during preparation of this manuscript. Funding for this work was in part provided by NIH Grants GM070555, GM 62999-1 and AHA to JJY.

Appendix A. Supplementary material

Supplementary data associated with this article can be found, in the online version, at doi:10.1016/j.jinorgbio.2008.06.014.

References

[1] J.A. Ibers, R.H. Holm, Science 209 (1980) 223–235.
[2] R.H. Holm, P. Kennepohl, E.I. Solomon, Chem. Rev. 96 (1996) 2239–2314.
[3] J.A. Tainer, V.A. Roberts, E.D. Getzoff, Curr. Opin. Biotechnol. 3 (1992) 378–387.
[4] J.P. Glusker, Adv. Protein Chem. 42 (1991) 1–76.
[5] J.R.R.F.D. Silva, R.J.P. Williams, The Biological Chemistry of the Elements: The Inorganic Chemistry of Life, Clarendon Press; Oxford University Press, Oxford [England], New York, 1991.
[6] S.J. Lippard, J.M. Berg, Principles of Bioinorganic Chemistry, University Science Books, Mill Valley, California, 1994.
[7] M.M. Yamashita, L. Wesson, G. Eisenman, D. Eisenberg, Proc. Natl. Acad. Sci. USA 87 (1990) 5648–5652.
[8] S.C. Bagley, R.B. Altman, Protein Sci. 4 (1995) 622–635.
[9] M. Babor, H.M. Greenblatt, M. Edelman, V. Sobolev, Proteins 59 (2005) 221–230.
[10] T. Dudev, C. Lim, Chem. Rev. 103 (2003) 773–787.
[11] T. Dudev, Y.L. Lin, M. Dudev, C. Lim, J. Am. Chem. Soc. 125 (2003) 3168–3180.
[12] H. Einspahr, C.E. Bugg, H. Sigel, Calcium and its role in biology, in: M. Dekker (Ed.), Crystal Structure Studies of Calcium Complexes and Implications for Biological Systems, 17, New York, 1984, pp. 52–97.
[13] M.M. Harding, Acta Crystallogr. D: Biol. Crystallogr. 55 (1999) 1432–1443.
[14] M.M. Harding, Acta Crystallogr. D: Biol. Crystallogr. 56 (2000) 857–867.
[15] O. Herzberg, J. Moult, M.N. James, J. Biol. Chem. 261 (1986) 2638–2644.
[16] K.C. Holmes, D. Popp, W. Gebhard, W. Kabsch, Nature 347 (1990) 44–49.
[17] E. Carafoli, J. Hypertens. Suppl. 12 (1994) S47–S56.
[18] L. Santella, E. Carafoli, Faseb J. 11 (1997) 1091–1109.
[19] R. Martin, Bioinorganic Chemistry of Calcium, Marcel Dekker, New York, 1984.
[20] M.R. Nelson, W.J. Chazin, Protein Sci. 7 (1998) 270–282.
[21] M. Tajima, I. Urabe, K. Yutani, H. Okada, Eur. J. Biochem. 64 (1976) 243–247.
[22] S. Forsen, E. Thulin, H. Lilja, FEBS Lett. 104 (1979) 123–126.
[23] J.S. Mills, J.D. Johnson, J. Biol. Chem. 260 (1985) 15100–15105.
[24] C.L. Wang, P.C. Leavis, J. Gergely, Biochemistry 23 (1984) 6410–6415.
[25] E. Pidcock, G.R. Moore, J. Biol. Inorg. Chem. 6 (2001) 479–489.
[26] W. Yang, A.L. Wilkins, Y. Ye, Z.R. Liu, S.Y. Li, J.L. Urbauer, H.W. Hellinga, A. Kearney, P.A. van der Merwe, J.J. Yang, J. Am. Chem. Soc. 127 (2005) 2085–2093.
[27] S.H. Chao, Y. Suzuki, J.R. Zysk, W.Y. Cheung, Mol. Pharmacol. 26 (1984) 75–82.
[28] C. Ferguson, M. Kern, G. Audesirk, Neurotoxicology 21 (2000) 365–378.
[29] S.H. Chao, C.H. Bu, W.Y. Cheung, Arch. Toxicol. 69 (1995) 197–203.
[30] Y. Suzuki, S.H. Chao, J.R. Zysk, W.Y. Cheung, Arch. Toxicol. 57 (1985) 205–211.
[31] E. Habermann, K. Crowell, P. Janicki, Arch. Toxicol. 54 (1983) 61–70.
[32] M. Kern, M. Wisniewski, L. Cabell, G. Audesirk, Neurotoxicology 21 (2000) 353–363.
[33] L.S. Busenlehner, D.P. Giedroc, J. Inorg. Biochem. 100 (2006) 1024–1034.
[34] K. Fahmy, M. Merroun, K. Pollmann, J. Raff, O. Savchuk, C. Hennig, S. Selenska-Pobell, Biophys. J. 91 (2006) 996–1007.
[35] J. Ye, A. Kandegedara, P. Martin, B.P. Rosen, J. Bacteriol. 187 (2005) 4214–4221.
[36] B. Borremans, J.L. Hobman, A. Provoost, N.L. Brown, D. van Der Lelie, J. Bacteriol. 183 (2001) 5651–5658.
[37] I. Hernandez-Ochoa, G. Garcia-Vargas, L. Lopez-Carrillo, M. Rubio-Andrade, J. Moran-Martinez, M.E. Cebrian, B. Quintanilla-Vega, Reprod. Toxicol. 20 (2005) 221–228.
[38] P. Apostoli, A. Bellini, S. Porru, L. Bisanti, Am. J. Ind. Med. 38 (2000) 310–315.
[39] C. Despres, A. Beuter, F. Richer, K. Poitras, A. Veilleux, P. Ayotte, E. Dewailly, D. Saint-Amour, G. Muckle, Neurotoxicol. Teratol. 27 (2005) 245–257.
[40] C.S. Chetty, G.R. Reddy, K.S. Murthy, J. Johnson, K. Sajwan, D. Desaiah, Int. J. Toxicol. 20 (2001) 113–120.
[41] G.R. Reddy, N.H. Zawia, Int. J. Dev. Neurosci. 18 (2000) 791–795.
[42] M.R. Moore, A. Goldberg, A.A. Yeung-Laiwah, Ann. N.Y. Acad. Sci. 514 (1987) 191–203.
[43] W.D. Atchison, J. Bioenergy Biomembr. 35 (2003) 507–532.
[44] S.H. Chao, C.H. Bu, W.Y. Cheung, Arch. Toxicol. 64 (1990) 490–496.
[45] J. Markovac, G.W. Goldstein, Nature 334 (1988) 71–73.
[46] C.M. Bouton, L.P. Frelin, C.E. Forde, H. Arnold Godwin, J. Pevsner, J. Neurochem. 76 (2001) 1724–1735.
[47] R.J. Andersen, R.C. diTargiani, R.D. Hancock, C.L. Stern, D.P. Goldberg, H.A. Godwin, Inorg. Chem. 45 (2006) 6574–6576.
[48] M.M. Harding, Acta Crystallogr. D: Biol. Crystallogr. 60 (2004) 849–859.
[49] J. Koca, C.G. Zhan, R.C. Rittenhouse, R.L. Ornstein, J. Comput. Chem. 24 (2003) 368–378.
[50] P.T. Erskine, N. Senior, S. Awan, R. Lambert, G. Lewis, I.J. Tickle, M. Sarwar, P. Spencer, P. Thomas, M.J. Warren, P.M. Shoolingin-Jordan, S.P. Wood, J.B. Cooper, Nat. Struct. Biol. 4 (1997) 1025–1031.
[51] E.K. Jaffe, J. Martins, J. Li, J. Kervinen, R.L. Dunbrack Jr., J. Biol. Chem. 276 (2001) 1531–1537.
[52] J.S. Magyar, T.C. Weng, C.M. Stern, D.F. Dye, B.W. Rous, J.C. Payne, B.M. Bridgewater, A. Mijovilovich, G. Parkin, J.M. Zaleski, J.E. Penner-Hahn, H.A. Godwin, J. Am. Chem. Soc. 127 (2005) 9495–9505.
[53] J.J. Yang, A. Gawthrop, Y. Ye, Protein Pept. Lett. 10 (2003) 331–345.
[54] M.R. Nelson, E. Thulin, P.A. Fagan, S. Forsen, W.J. Chazin, Protein Sci. 11 (2002) 198–205.
[55] N.C. Strynadka, M.N. James, Annu. Rev. Biochem. 58 (1989) 951–998.
[56] K.L. Yap, J. Kim, K. Truong, M. Sherman, T. Yuan, M. Ikura, J. Struct. Funct. Genomics 1 (2000) 8–14.
[57] C.S. Fullmer, S. Edelstein, R.H. Wasserman, J. Biol. Chem. 260 (1985) 6816–6819.
[58] H. Ouyang, H.J. Vogel, Biometals 11 (1998) 213–222.
[59] R.H. Kretsinger, C.E. Nockolds, J. Biol. Chem. 248 (1973) 3313–3326.
[60] Y. Zhou, W. Yang, M. Kirberger, H.W. Lee, G. Ayalasomayajula, J.J. Yang, Proteins 65 (2006) 643–655.
[61] H. Kawasaki, S. Nakayama, R.H. Kretsinger, Biometals 11 (1998) 277–295.
[62] G. Sarret, A. Manceau, L. Spadini, J.C. Roux, J.L. Hazemann, Y. Soldo, L. Eybert-Berard, J.J. Menthonnex, Environ. Sci. Technol. 32 (1998) 1648–1655.
[63] M.M. Harding, Acta Crystallogr. D: Biol. Crystallogr. 58 (2002) 872–874.
[64] A.L. Swain, R.H. Kretsinger, E.L. Amma, J. Biol. Chem. 264 (1989) 16620–16628.
[65] D.W. Cruickshank, Acta Crystallogr. D: Biol. Crystallogr. 55 (1999) 583–601.
[66] W.L. DeLano, The PyMOL Molecular Graphics System, 2002.
[67] B.J. Marsden, G.S. Shaw, B.D. Sykes, Biochem. Cell Biol. 68 (1990) 587–601.
[68] H.A. Godwin, Curr. Opin. Chem. Biol. 5 (2001) 223–227.
[69] G. Battistuzzi, M. Borsari, L. Menabue, M. Saladini, M. Sola, Inorg. Chem. 35 (1996) 4239–4247.
[70] L. Shimoni-Livny, J.P. Glusker, C.W. Bock, Inorg. Chem. 37 (1998) 1853–1867.
[71] W. Yang, H.W. Lee, H. Hellinga, J.J. Yang, Proteins 47 (2002) 344–356.
[72] S. Linse, P. Brodin, C. Johansson, E. Thulin, T. Grundstrom, S. Forsen, Nature 335 (1988) 651–652.
[73] S. Linse, S. Forsen, Adv Second Messenger Phosphoprotein Res. 30 (1995) 89–151.
[74] W. Yang, L.M. Jones, L. Isley, Y. Ye, H.W. Lee, A.L. Wilkins, Z.R. Liu, H.W. Hellinga, R. Malchow, M. Ghazi, J.J. Yang, J. Am. Chem. Soc. 125 (2003) 6165–6171.
[75] M.A. Wilson, A.T. Brunger, Acta Crystallogr. D: Biol. Crystallogr. 59 (2003) 1782–1792.
[76] B. Honig, A. Nicholls, Science 268 (1995) 1144–1149.
[77] W. Rocchia, E. Alexov, B. Honig, J. Phys. Chem. B 105 (2001) 6507–6514.
[78] M.K. Gilson, B. Honig, Proteins 4 (1988) 7–18.
[79] A. Nicholls, B. Honig, J. Comput. Chem. 12 (1991) 435–445.
[80] L. Willard, A. Ranjan, H. Zhang, H. Monzavi, R.F. Boyko, B.D. Sykes, D.S. Wishart, Nucleic Acids Res. 31 (2003) 3316–3319.
[81] C.A. McPhalen, N.C. Strynadka, M.N. James, Adv. Protein Chem. 42 (1991) 77–144.
[82] I.A. Bergdahl, A. Grubb, A. Schutz, R.J. Desnick, J.G. Wetmur, S. Sassa, S. Skerfving, Pharmacol. Toxicol. 81 (1997) 153–158.
[83] S.N. Kelada, E. Shelton, R.B. Kaufmann, M.J. Khoury, Am. J. Epidemiol. 154 (2001) 1–13.
[84] P.T. Erskine, E.M. Duke, I.J. Tickle, N.M. Senior, M.J. Warren, J.B. Cooper, Acta Crystallogr. D: Biol. Crystallogr. 56 (2000) 421–430.
[85] Y. Wang, L. Hemmingsen, D.P. Giedroc, Biochemistry 44 (2005) 8976–8988.